RSC Advances

ROYAL SOCIETY OF CHEMISTRY

www.rsc.org/advances

A novel third generation xanthine biosensor with enzyme modified glassy carbon electrode using electrodeposited MWCNT and nano-gold polymer composite film

Sarani Sen, Priyabrata Sarkar*

Sensor Laboratory, Department of Polymer Science and Technology,

University of Calcutta, 92 APC Road, Kolkata 700009, India

Email: sarani.sen@gmail.com; sarkarpriya@gmail.com*

Ph: +913324852975

Fax: +91332351975

***Corresponding author**

Abstract

A novel nanobiocomposite for immobilization of xanthine oxidase (XO) was developed by incorporating functionalized MWCNT in nanogold doped poly(o-phenylenediamine)(PPD) (Au-PPD) film on glassy carbon electrode(GCE) for selective and sensitive detection of xanthine in real samples e.g. blood, urine, fish. Stable colloid of o-phenylenediamine(OPD) and $HAuCl_4$ in acidic environment was electropolymerized on working electrode(GCE) to form ultrathin film of AuNP-PPD which possessed permselectivity and no interference against electroactive species such as ascorbic acid and uric acid. Spectrophotometric and microscopic analysis confirmed the doping behaviour of AuNP. Electrodeposition of carboxylated MWCNT onto the Au-PPD film increased conductivity, sensitivity and also facilitated a microenvironment to entrap XO enzyme by covalent bonding enhancing storage stability. The conductive nature of the electrode after every step of modification was investigated by electrochemical impendence spectroscopy. High I_{max}/K_{map} value was achieved by XO/fMWCNT/Au-PPD modified electrode. Oxidation of xanthine on this modified electrode was diffusion-controlled involving two-electron in the rate-determining step with a transfer coefficient (α) of about 0.596. Differential pulse voltammetric study of XO/fMWCNT/Au-PPD/GCE exhibited good analytical characteristics e.g. low detection limit (12nM) (S/N=3), a wide linear range of 0.01-300 μM (R^2=0.994), good sensitivity (14.03 μA $\mu M^{-1} cm^{-2}$), fast response (6s) at anodic potential of +0.625V vs. Ag/AgCl (pH 7.0). It retained 91% of its initial activity even after 210 times of use over a period of 4 months when stored at 4°C. The applicability of the xanthine biosensor was tested by performing reproducibility, repeatability and interference study on real samples.

Keywords: Xanthine; Xanthine oxidase; Biosensing; differential pulse voltammetry, electrochemical impedance spectroscopy.

1. Introduction

Freshness of fish, meat and other derived products is a prime requirement for human health. There is worldwide demand for reliable, handheld analytical tool to monitor freshness of fish and meat. When animal tissue dies, ATP degrades to xanthine and the pathway is: ATP>ADP>AMP>IMP>HxP>Hx>X.[1] Thus the levels of xanthine in fish product can be used as an index for evaluating meat or fish freshness.[1,2] Determination of xanthine level in blood, urine tissue is also essential for medical diagnosis and management of various diseases such as hyperuricemia, gout, xanthinuria and renal failure.[3] Development of a xanthine sensor is thus of immense importance in food, medical and biological research.[4] Xanthine oxidase (EC:1.17.3.2, XO), the metalloflavoprotein is a key enzyme at the end stage of protein degradation during hydroxylation of purines in the 2, 6, and 8 ring positions to form purine followed by hypoxanthine/ xanthine and finally uric acid. Biosensors, in general, show greater sensitivities compared to traditional physicochemical, biological and serological tests based on UV/vis spectrophotometry, high performance liquid chromatography, gas chromatography.[5,6] Electrochemical biosensors combine the advantages of the specificity of the enzyme for recognizing particular target molecules with direct transduction of the rate of reaction into a current. Since biomolecules used in biosensing are not conducting in nature, conducting microenvironments are required to transfer the electrons from active site of the enzyme to electrode surface.[7-9] The sensitivity of biosensor mainly depends on the conductivity, nature of entrapment matrix for enzyme immobilization on the electrode.

A support of polymeric matrix enhances speed, sensitivity and versatility in diagnostics of target analytes. Conducting polymers such as polyaniline (PANI), polypyrole (PPy) and

poly[3,4-ethylenedioxythiophene] (PEDOT) have been used for biosensing of xanthine, glucose, uric acids.[4,7,10-13] Although, o-phenylenediamine (OPD) is an aniline derived polymer with an extra $–NH_2$ group, the oxygen reduction ability at PPD film (in reduced state) is unique compared to PANI, PPy [Gajendran 2007].[14] The excellent permselectivity properties of electropolymerized poly(o-phenylenediamines (PPD) have wide application for designing oxidase-based biosensors due to highly permeability to H_2O_2 and efficient blockers of interference compounds.[15-17] Nanoparticles such as Au, Ag, Pt, ZnO, Fe_3O_4 have attracted enormous interest in the past years due to their superior role in acceleration of the electron transfer rate from enzyme to working electrode.[4,15,18-20] The main advantages of gold nanoparticles (AuNP) used in biosensing applications are nontoxicity, good biocompatibility, high electron communication rate. Thus the application of AuNP could be useful in biosensing replacing external electron-transfer mediators.[18,20] It was demonstrated that polyaniline (PANI), polypyrrole (PPy),PANI–PPy copolymers, poly(3,4-ethylene dioxythiophene) (PEDOT), poly-(phenylene vinylene) (PPV) and several other conducting polymers (CPs) could spontaneously reduce noble metal ions (e. g Ag^+, Au^{3+}, Pd^{2+}, and Pt^{2+}) to zero valent metals.[7,19-21] Conducting polymers have been used as supporting matrix for intercalation of important nanoparticles to retain the catalytic activity of enzymes in the composite.[7,19,22] However, ultrathin Au doped PPD film (Au@PPD) through a single step electrodeposition of Au-PPD nanocomposite has not been reported in literature.

In recent years, carbon derivatives such as carbon nanotubes (CNT), graphite and graphene have been used for their unique electrical, mechanical, structural and chemical properties. The potential use of functionalized MWCNT for biosensing applications have shown great promise for diagnosis of trace molecules due to its excellent electrical conductivity, ultra

high mechanical strength, good chemical stability, high specific area and high dimensional ratios.[8,9,14,23-24] In last few years, a few reports were published on electrochemical xanthine biosensor. The comparison of performances of some well characterized xanthine biosensors is given in Table 1.[22-31] Most of these suffered from lower storage stability, non-reusability, high time of response, low electron transfer rate and complexity of fabrication process.[4,10,20,23-31] The complexity of the enzyme entrapment was against the acceptability for commercial use. The lack of storage stability due to leaching of enzymes could be overcome by covalent linkage of enzyme to the electrode surface and the main aim of our study concentrated on fabrication of a highly stable and sensitive xanthine biosensor with low detection limit.

A new design of sensing matrix using the favourable effect of conducting nature of OPD, AuNP and fMWCNT matrix was used for entrapment of XO for detection of xanthine in real samples. Incorporation of AuNP in PPD film formed an ultrathin, adherent layer on which a further electrodeposition of carboxylated MWCNT was made. XO could successfully bind with activated –COOH group of fMWCNT without altering the enzyme activity. In many publications amperometric xanthine biosensors have been reported and these were based on the cyclic voltammetry (CV) i.e current measurements at fixed applied potential[4,23-31] whereas differential pulse voltammetry (DPV) could have been a better measurement technique due to sharper response peaks i,e., higher sensitivity. In the present research DPV based analysis showed higher sensitivity and selectivity for xanthine in real samples such as human blood serum, urine as well as fish.

Table 1 Analytical characteristics of some recently developed xanthine oxidase based biosensor for detection of xanthine.

Reference	Electrode modification	Method of immobilization	Eapp vs Ag/AgCl / technique	Optimum pH	Linear range (μM)	Detection limit (μM)	Sensitivity	Response time(s)	Storage stability (%)	Analyte/ Applications
[26]	XO–Au-np–GCPE		0.70V / amp	7.5	0.5-10	-	0.24 μA μM^{-1}	-	7days (72% retain)	X/ Hx
[27]	XO/laponite	Physico-adsorption	0.39V / amp	7.5	0.039-21	0.01	6.54 mA M^{-1}			
[23]	XO/ZnO-NP/CHIT/c-MWCNT/PANI/PtE	covalently	0.050V / amp	7.0	0.1–100	0.1	-	4	1month (70% retain after 80 uses)	X/ fish
[10]	GMC/GCE	-	0.65 V / dpv	7.0	20–320	0.388	0.062 μA μM^{-1}	-	-	UA, X, Hx/ fish, blood, urine
[28]	Naf/XO-CD/pAuNP/SWNT/GCE	Physicoadsorption	0.65 V / amp	7.0	0.05−9.5	0.04	0.152 μA μM^{-1}	-	-	-
[29]	XO/GNPs–SWCNT/PtE	Physicoadsorption	0.4V / amp	7.4	2000-37300	0.61	0.141 μA μM^{-1}	-	2week (88% retain)	-
[30]	XO/CHIT/Fe-NPs@Au/**PGE**	Covalent glutaraldehyde	0.5V /amp	7.4	0.1–300	0.1	1.169 μA μM^{-1}	-	100 days (25% loss)	X/ fish
[31]	XOD/CHT/PtNPs/PANI/Fe3O4/CPE	Covalent glutaraldehyde	–0.35 V /amp		0.2 - 36	0.1	13.58μAμ M^{-1} cm^{-2}	-	3 month (85% retain after 100 uses)	-
[24]	P(GMA-co-VFc)/MWCNT/XO	Physico-adsorption	0.35V / amp	7.0	2–48	0.12	16 mA M^{-1}	4	25days (70%retain)	X/ fish
This work	XO/fMWCNT/Au-PPD/GCE	Covalent	0.625 V / dpv	7.0	0.01-300	0.012	14.03 μA μM^{-1} cm^{-2}	5	4months (91% retain after 210 uses)	X / fish blood, urine

GCPE : Glassy carbon paste electrode; CD- Cyclodextrin; CHIT- Chitosan; SWCNT- Single walled carbon nanotube; PtE-Platinum electrode; PGE- Pencil graphite electrode; CPE- Carbon paste electrode; X- Xanthine, Hx-Hypoxanthine, Naf- Nafion; GMA-co-VFc- poly(glycidyl methacrylate-co-vinylferrocene)

2. Experimental Methods

2.1 Chemicals and Apparatus

Multiwall carbon nanotubes (MWCNT), o-phenylenediamine (OPD), xanthine oxidase (XO,E.C.1.1.3.22 from microorganism), gold chloride salt ($HAuCl_4$. $3H_2O$) were purchased from Sigma Aldrich, USA. 1-ethyl-3-(3-dimethylaminopropyl)carbodiimidehydrochloride (EDC), N-hydroxysuccinamide (NHS), xanthine(Xn), hypoxanthine (HyX), uric acid (UA) were obtained from Himedia, India. Potassium di-hydrogen phosphate (KH_2PO_4) and di-potassium hydrogen phosphate (K_2HPO_4), sodium sulphate (Na_2SO_4), L-ascorbic acid (AA), hydrogen chloride acid, nitric acid, sulphuric acid, perchloric acid were procured from E-merck (Mumbai, India). Three electrode system having glassy carbon working electrode (WE), Ag/AgCl reference electrode (RE) and platinum (Pt) counter electrode (CE) were used for all electrochemical analysis. The electrochemical measurements were conducted using IVIUMStat electrochemical analyzer (Model: A09050, Iviumstat Technologies, USA) with IviumSoft software. Electrochemical impendence spectroscopy (EIS) was performed at each step of electrode modification using frequency response analyser (Eco Chemie B.V, Utrecht, Netherlands) attached with Autolab, AUT72660 and controlled by FRA 4.9.006 software. EIS study of the modified electrodes was carried out in 5mM of $[Fe(CN)6]_3^-$ and $[Fe(CN)6]_4^-$ with 0.1M KCl at frequency range 1MHz to 0.01 Hz, amplitude 10mV and fixed potential of 0.28V. The detailed measurement procedure for SEM, FESEM, TEM, FTIR, XRD, EDAX is given in supporting information.

2.2 Carboxylation of MWCNT

Functionalization of commercial MWCNT (average dia ~50nm) was the most important step in sensor fabrication. 20mg of commercially available MWCNT was dispersed in 4M HCl for 2 hours with the aid of ultrasonic agitation to eliminate metal oxides that are catalyzed within the MWCNT.[32-33] The separated MWCNT was rinsed with RO water until the pH became neutral. The dried MWCNT then was dispersed in 24 ml of a mixture of concentrated HNO_3 and H_2SO_4 (1:3 v/v) with constant stirring of 1h at 50^oC followed by sonication for 2h in ultrasonic bath with alternative 10min of stirring to get functionalized and shortened fMWCNT. The fMWCNT was separated by centrifugation at 10000 rpm for 10 min. The pellet of fMWCNT, was washed with deionized water several times and neutralized by 1M NaOH until neutralized. Finally it was centrifuged at 10000 rpm for 10min to collect the fMWCNT. The pellet was dried overnight in a hot air oven.

2.3 Fabrication of modified electrode

Three-electrode assembly was used for all the electrochemical experiments. The glassy carbon working electrode and platinum counter electrode were first cleaned with polishing kit. The electrodes were washed with RO water thoroughly after sonication in ethanol/water mixture for five minutes, and then cleaned electrochemically by cyclic voltammograms of 5 cycles (-0.5 to 1.5 V) in 0.5 M sulphuric acid. Stable Au/o-PD colloidal solution was prepared by drop wise addition of 1mM auric chloride into the 0.08M OPD monomer solution in 0.1 M HCl and 0.1 M Na_2SO_4 under continuous stirring for 10 min. Au doped thin conducting polymeric film of OPD was electrodeposited on GCE by cyclic voltammetry (CV) in the potential span of -0.4V to 1.4V at scan rate 0.05V/s for 20 cycles in Au/o-PD colloidal solution. A bluish green ultra thin layer of Au doped PPD film was formed onto the shiny surface of GCE. The unbound monomer was

removed further by chronoamperometry at -0.2V for 10 minutes in deionized water. 0.05% (w/v) fMWCNT was sonicated in deionized water for 10 min before electrodeposition onto the Au-PPD modified GCE surface. The chronoamperometric electrodeposition was performed at 1.7V for 30 min to construct fMWCNT/Au-PPD/GCE. The surface coverage by the fMWCNT was calculated to be 2.78X 10^{-6} mol cm^{-2}. The fMWCNT on the electrode surface was further activated by EDC-NHS. The same was first stirred for 30 minutes in 10mM EDC in phosphate buffer (50mM, pH 7.0) and 10mM NHS was then added and stirred for further 1 hour to form a stable NHS-carbodiimide-ester onto the surface of fMWCNT. The modified electrode was washed thrice with buffer to remove nonspecific chemicals. Finally 0.1U of XO enzyme was adsorbed covalently with activated fMWCNT onto the electrode surface to construct a unique mediator free design of XO/fMWCNT/Au-PPD/GCE. The –COOH groups of fMWCNT was linked covalently to $–NH_2$ groups of XO which provided a more stable complex than physical aggregation. A schematic diagram of stepwise electrode fabrication of the proposed XO/fMWCNT/Au-PPD/GCE sensor is shown in Scheme I.

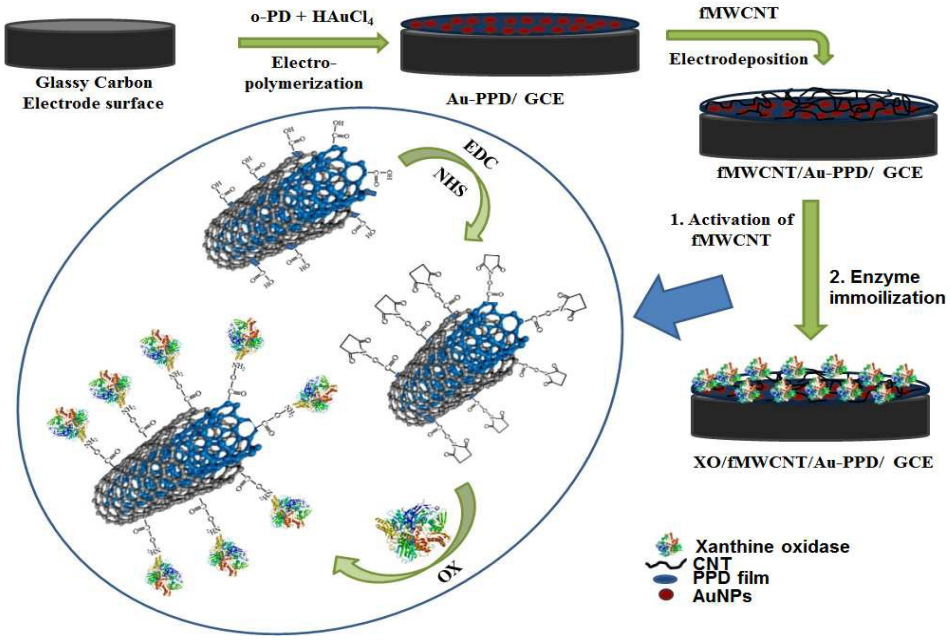

Scheme I. Fabrication steps for a unique design of enzyme electrode namely XO/fMWCNT/Au-PPD/GCE

Variation in fabrication process was considered to evaluate the best design for xanthine biosensor which could provide higher stability and sensitivity. To look into the effect of Au doped PPD, only PPD film was electropolymerized onto the bare GCE in absence of auric chloride with same electropolymerization conditions to construct PPD/GCE and kept aside. A layer of AuNP was electrodeposited by chronoamperometry at -0.273V in 1mM chloroauric solution onto another PPD/GCE modified electrode to form Au/PPD/GCE. To evaluate the change in response with nafion coverage, an electrode was modified to construct Naf/XO/fMWCNT/Au-PPD/GCE. All enzyme modified electrodes were stored in buffer (50mM, pH 7) at 4◦C until further use. Table 2 shows the response due to variation in fabrication.

2.4 Sample preparation

Three different samples were tested. The fish samples e.g. *Lebeo rohita* (F1) and *Lates calcarifer* (F2) were purchased from local market, Kolkata. The fish extract was prepared by following published report.[20,23,30] 1gm of fish flesh was converted into a fine paste using 5ml of 0.5M perchloric acid ($HClO_4$) by a motor pastel. The extract was stirred mechanically for 10 min to make a homogenized mixture. Centrifugation was then performed at 6000 rpm for 15min. the supernatant was collected and neutralized by drop wise addition of 0.6 M NaOH. Blood serum and urine samples were collected from a medical diagnostic centre in Kolkata, India (not collected directly from human volunteers). These were filtered through 0.45 micron membrane (Milli pore, India) before analysis. 50 µL of each sample was added to the electrochemical cell to

196 monitor the xanthine level in the real samples. The xanthine levels in real samples were also
197 quantified using C-18 HPLC column (Nova-Pak C18, 3.9×150 mm) with 5 µm pore size and a
198 binary pump system of WATERS 2487(Massachusetts, USA) by using mobile phase of
199 methanol:water:acetic acid (7.5:92:0.5 v/v/v) with 0.5 mL min^{-1} of flow rate at 272 nm. All
200 experiments were performed in compliance with the relevant laws and institutional guidelines.
201 Theinstitutional committee has also approved the experiments.

202 **3. Results and discussion**

203 *3.1 Electrochemical deposition of Au doped poly(o-phenylenediamine) [Au-PPD] on GCE*

204 Fig. 1 depicts the cyclic voltammetric growth profile of PPD and Au-PPD onto bare GCE
205 along 20 scans in the range of -0.4 to 1.4V. In the first cycle, a broad oxidation peak with 1.556
206 times higher anodic current appears at 0.74V for Au-PPD than only monomer oxidation (at
207 0.88V), indicating the faster formation of OPD radical cation through one electron oxidation of
208 amino group.[14] For both the electrodes, oxidation peak current decreased gradually. In case of
209 Au-PPD (Fig. 1b), the second scan produced two oxidation peaks at 0.67V and 1.01 V, both of
210 which diminished with number of scans. On the reverse scan, there were no corresponding
211 cathodic peaks, indicating that active cation radicals underwent polymerization reaction
212 immediately.[14] For the second scan another oxidation peak was observed at -0.08Vwith larger
213 peak current than only PPD, that decreased gradually till scan 5, after that two peaks appeared at
214 -0.11V and 0.01V with increasing current in the following scans, that was not observed for
215 polymerization of PPD. At the lower potential, two cathodic peaks at -0.14V and 0.04V merged
216 into one peak at -0.02V with continuous scan for monomer polymerization (Fig. 1a), whereas
217 two distinct peaks at -0.15V and -0.04V appeared with higher Ip value during formation of Au-

PPD film (Fig.1b). The increase in peak current of the redox pair at 0.11/-0.15V in presence of $HAuCl_4$ indicated successful incorporation of gold nano-cluster into the Au-PPD film. The thickness of the Au-PPD film was calculated to be 178.2±12nm using the equation $d=mQ/FA\rho$,[11] where, m denotes the molecular weight of the monomer; Q the electric charge during the electropolymerization; F the Faraday constant (F=96485 C mol^{-1}); A the surface area of the working electrode (i.e. 0.0707cm^2) and ρ the density of PPD. The ultrathin film of polymeric matrix could be synthesized only by electro-polymerization ensuring many advantages compared to other coating methods for enzyme based electrode fabrication: (i) high uniform polymeric matrix in a controllable manner for enzyme immobilization, (ii) fast electron transfer and mass transport, (iii) removal of intra-layer diffusion mass transport limitations. Thus supportive matrix for enzyme immobilization could remain constant in repeated synthesis during sensor fabrication. The surface coverage Γ of the electrode was evaluated by integrating anodic peak current, determining the average charge Q using Faraday's law [Eq.1][11] and was found to be 1.648X 10^{-9}±0.26 mol cm^{-2} for Au-PPD film, whereas surface coverage by only PPD film was calculated as 1.254X 10^{-9}±0.31 mol cm^{-2}.

$$\Gamma = Q/nFA \qquad (1)$$

Where n is the number of electrons transferred in redox reaction, the other symbols have their usual meaning.

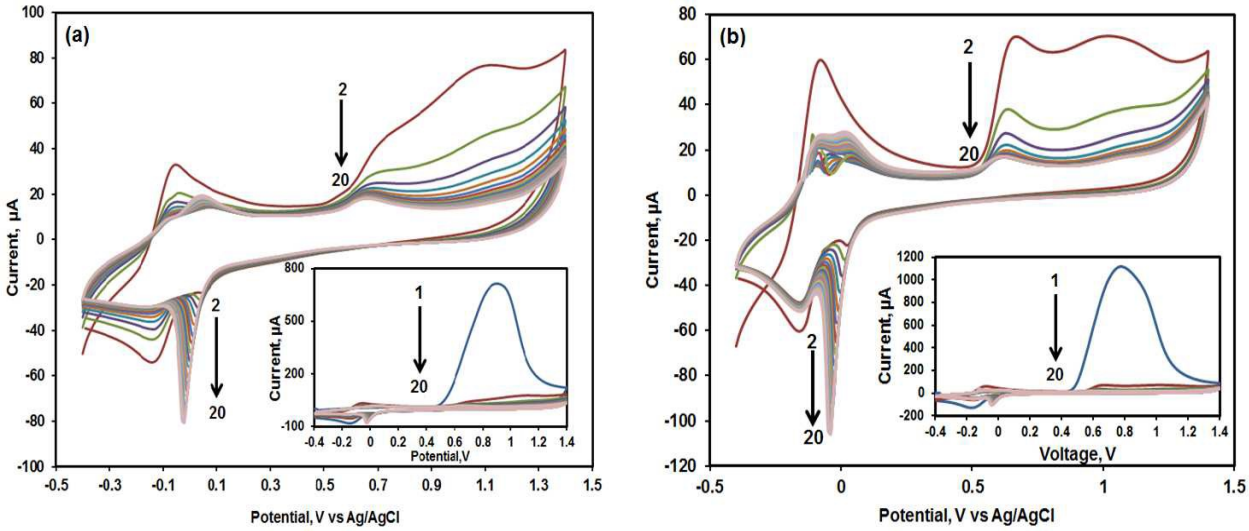

Fig. 1 Cyclic voltammogram during electropolymerization of Poly(o-phenylenediamine) in absence (a) and presence of $HAuCl_4$(b). Inset: change of CV patterns from scan 1 to 20. Conditions: scan rate: 0.05V s-1, potential range: -0.4 to 1.4, Electrodes: WE: bare *GCE, RE: Ag/AgCl, CE: Platinum wire*.

3.2 Spectrophotometric and microscopic characterization of Au doped PPD film

Scheme II represents the proposed chemical structure of Au doped PPD film that may be formed by electrochemical growth through head-to-head and/or head-to-tail coupling of OPD cation radicals. Delocalization of electron occurred between chains and neighbouring redox sites of polymer during oxidative or reductive electro-polymerization. Previous work ,[34,35] explained that electron rich N atom of amines had strong affinity towards electron deficient AuNP, which could be comparable to Au-S bond energy. OPD has two sp^2 nitrogen atoms in the aromatic amine ring, thus a strong N-Au bond may form easily. As a result, OPD can act as an oxidant in presence of auric chloride. Fig 2a displays a rapid color change from yellow to brown with addition of increasing concentration (0.01, 0.05, 0.1, 0.25, 0.5, 0.75, 1mM) of $HAuCl_4$

suggesting the formation of a stable Au-PPD colloidal solution by reduction of Au^{3+} to Au^0 and simultaneously chloride ions were incorporated during polymerization of OPD in acidic environment.[34] This phenomenon could be characterized by spectrophotometric analysis of the colloidal mixture before and after addition of $AuCl_4$. The UV/vis spectra are shown in Fig. 2a. The peak at 281nm could be assigned for π- π* transition of benzenoid ring.[36] Other peaks at 415, 451 and 474nm were observed after electro-oxidation of OPD and these were absent in the monomer. These peaks were gradually more pronounced with increase in concentration of Au doping due to the charge transfer excitation e.g. transition related to the benzoid unit in the reduced state of the polymer.[14,37] The peak at 451 appeared for phenazine-like dimers/oligomers formation by cyclization (internal coupling); the peak at 415 nm could be attributed for the intermediates of the dimeric or oligomeric species containing phenazine structure. The absorption bands at 474nm were assigned to the low intensity of cation radicals of aniline-type dimer that further was coupled to the PANI-like radical or its dicationic form.[38] The variation of fluorescence spectra also confirmed the interaction of gold nanoclusters to polymer that was depicted in Fig. 2c. Only PPD exhibited an emission peak at 466nm when excited at 395nm, whereas Au doped PPD showed two distinct maxima at 467nm and 567 nm in acidic environment. With the addition of $HAuCl_4$ from 0.01to 1mM, the emission peak intensity got enhanced at 566nm but subsequently decreased at 466nm gradually. Thus the new composite had shown unique physical characteristics owing to Au doping.

The FTIR spectra of OPD, PPD were compared with the Au doped PPD film that was synthesized onto the GCE surface in Fig. 2d. A typical IR spectrum profile of OPD with two peaks at 3384 $cm^{-1}$and 3362 cm^{-1} could be characterized for asymmetric and symmetrical N-H stretching vibrations, while the bands at 1271.44 cm^{-1}, 1154.74 cm^{-1}, 1057.77 cm^{-1} could be

ascribed for C-N stretching vibrations. The two bands at 1497.7 cm^{-1} and 1456.96 cm^{-1} corresponded to C=C stretching vibrations of benzenoid rings, and shifted after electropolymerization. An IR band of OPD at 3384cm^{-1} was due to the presence of primary amine that changed into N-H bending of secondary amine at 1504 cm^{-1} in the PPD film during electropolymerization. The IR spectrum of PPD and Au doped PPD was nearly the same indicating no structural changes during polymerization. A ladder polymeric chain of PPD was characterized by the following peaks at 3405, 1628, 1537, 1315 might be ascribed to N-H, C=N, C=C, C-N stretching vibration of phenazine structures in PPD respectively.[14,36-39] Two other peaks at 977 and 761 cm-1 could be attributed to the out of plane C-H bending vibrations of aromatic benzene with the phenazine skeleton.[36-39] The peak intensity of the IR band for sulphate dopant at 1093 cm^{-1} increased in presence of AuNP of PPD film. Since, incorporation of AuNP did not change the IR band position of Au-PPD film, successful electrodeposition of Au doped PPD film could be predicted. A shift of 2 cm^{-1} for the sulphate group stretching at 1092cm^{-1} in presence of AuNP in PPD film was likely due to a change in their dipole moment when AuNP got bound to the surface of high electron density.

Spherical deposition of nanoclusters of AuNP was observed clearly in SEM and FESEM image of Au doped PPD film (Au-PPD) in Fig. 2e-f respectively, that was not observed for only PPD film (image not shown). The TEM image in Fig. 2e, also clearly showed that spherical AuNPs (4-16nm)(11.2±4.5) were mono dispersed as well as nanoclustered in the Au-PPD film and EDAS spectra (Fig. 2g) confirmed the presence of AuNP in Au-PPD film. The electron diffraction (SAED) pattern of thin film displayed polycrystalline diffraction rings with bright spots that particularly represented well orientations of microcrystals (Fig. 2b) in a number of different directions. The crystalline property of Au-PPD thin film was characterized by XRD, as

shown in S-Fig 1. A number of Bragg reflections with 2θ values of 22.91°, 28.38°, 32.91°, 38.68°, 45.84°, 55.27° and 61.78° were observed. Several main peaks centred at 2θ= 22.91°, 28.38°, 32.91° were characterized for doped PPD, corresponding to the periodically parallel and perpendicular chains of the polymer matrix.[39] The familiar peaks appearing at 2θ values of 38.68°, 45.84°, 55.27°, 61.78° were for the (111), (200), (220) and (311) sets of lattice planes respectively depicting the face centred cubic (fcc) structure of gold nanocrystals.

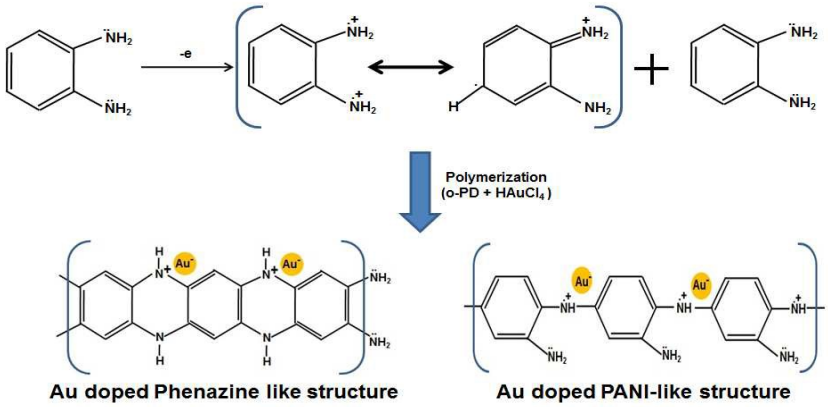

Scheme II. The proposed mechanism of electrochemical growth of Au doped PPD film

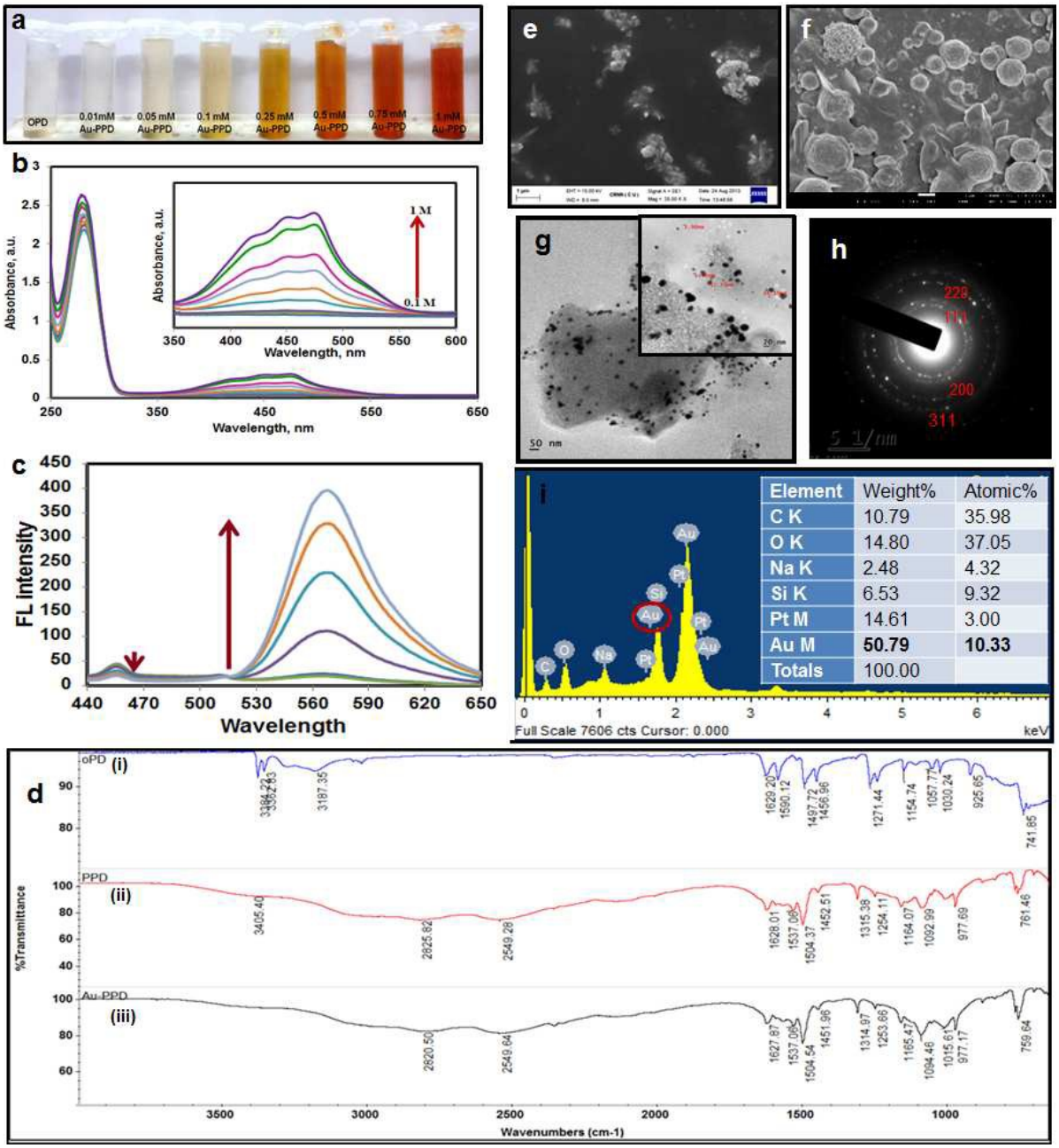

Fig. 2 (a) Change of color profile due to addition of 0 to 1mM auric chloride salt; (b) Change of UV/Vis spectra pattern for Au doped PPD, inset: increasing peak intensity pattern for addition of 0,0.01,0.05,0.1,0.25,0.5,0.75,1mM $AuCl_4^-$; (c) Fluorescence spectra for increasing concentration (0-1mM) of Au doping in PPD film; (d) FTIR spectra of OPD monomer (i), PPD (ii), Au doped

PPD (iii); (e & f) SEM and FESEM image of Au-PPD respectively; (g) TEM image of Au-PPD, inset showed the HRTEM image of the selected area of (g); (h) diffraction pattern of Au-PPD showing crystallinity of AuNP; (i) EDAX of Au-PPD film.

3.3 Functionalization of MWCNT

Functionalization of as-received MWCNT was a crucial step for formation of a uniform suspension before electrochemical deposition (Fig. 3a). After acid treatment, abundantly negative charged MWCNT provided a microenvironment to form a uniform stable water suspension through electrostatic interaction (Fig. 3b). In the FTIR spectra (Fig. 3c), several drastically enhanced absorption peaks in the range of 3400-3800 cm^{-1} were observed in the fMWCNT, compared to commercial MWCNT, confirming the presence of –OH group onto the backbone of fMWCNT. Two peaks at 3485 and 1660 cm^{-1} were due to the O-H stretching vibration and C=O vibrations of carboxylic group respectively, indicating a successful incorporation of –COOH to the end or sidewalls of the MWCNT. Fig 3d shows the FESEM image of fMWCNT. From the TEM images, it could be clearly observed that the fMWCNT became shortened and thinner (Fig. 3f-g) during acid treatment compared to the as-received MWCNT (Fig. 3e). The average diameter of the fMWCNT was reduced to 18.36±7.35 nm. Fig. 3g displays the defects of the side walls of the nanotubes due to chemical oxidation by strong acids. This defect increased the reactivity due to presence of functional groups on its surface. Two XRD peaks at 2Θ of 25^{o}, 42^{o} were changed after functionalization. The crystallization pattern was altered to 2theta values of 28^{o}, 33^{o}, 48^{o}, 54^{o}, 59^{o}, 73^{o} confirming the carboxylation of MWCNT (S-Fig. 2a). EDAX spectra of fMWCNT (S-Fig. 2b) also confirmed the presence of oxygen on the surface of fMWCNT.

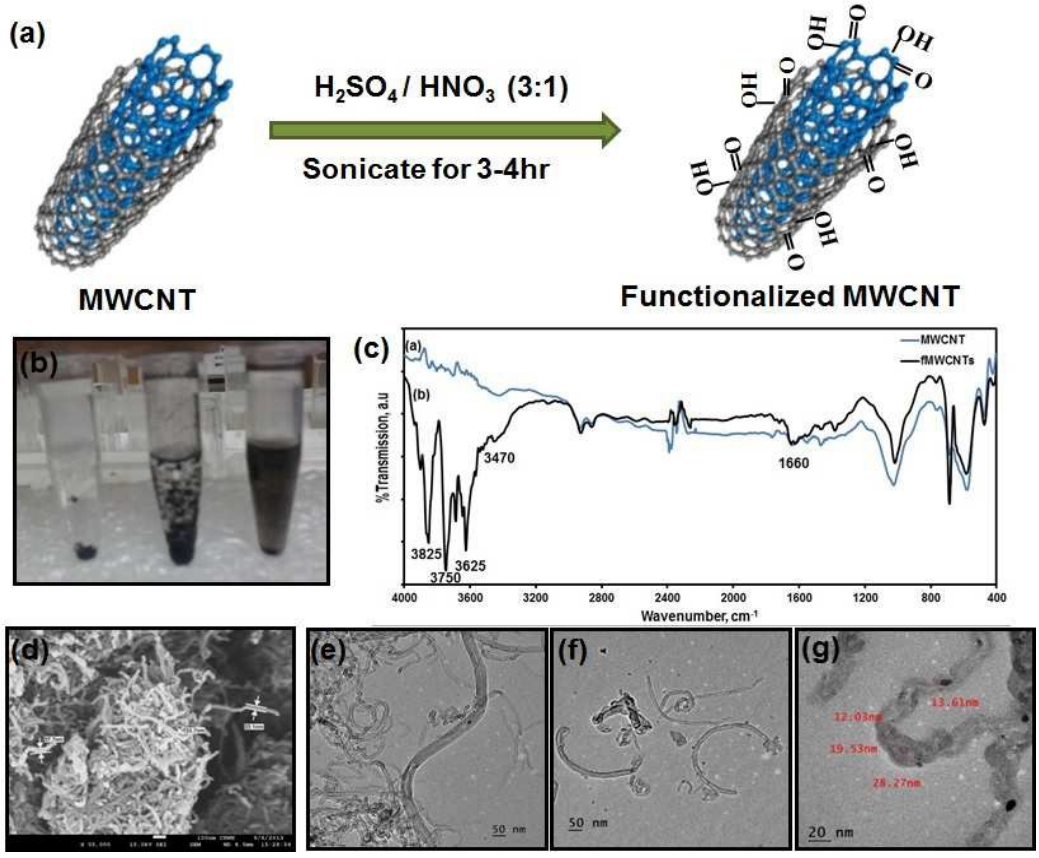

Fig 3 (a) A schematic diagram on functionalization of MWCNT; (b) the eppendorf tubes show the increase rate of solubility of FMWCNT after acid treatment, (c) change of FTIR spectra for functionalized MWCNT, (d) FESEM and (e) TEM images of MWCNT; (f,g) TEM image of fMWCNT;

3.4 Electrochemical kinetic studies for xanthine determination and data Analysis

Different immobilization designs (already mentioned in section 2.3) were followed to achieve optimum catalytic activity of enzyme. To evaluate the catalytic properties of electrodes to the oxidation of xanthine, characteristic CVs were recorded (Fig.4) in the potential range of 0.3 to 1.0V with a scan rate of 50mV s^{-1}. Fig. 4 shows the CVs of XO/PPD/GCE (a), XO/Au-PPD/GCE(b), XO/fMWCNT/Au-PPD/GCE(c), and Naf/XO/fMWCNT/Au-PPD/GCE(d) in 0.05

M Potassium phosphate buffer containing 50µM xanthine respectively. As can be seen in Fig. 4, the responses of XO/PPD/GCE, XO/Au-PPD/GCE towards xanthine are very weak, might be due to the very slow electrode kinetics. It was observed that the anodic peak current at 0.65V was enhanced 42 fold after incorporation of fMWCNT on Au-PPD film, whereas, it could decrease 1.5 times due to outer layer coating of nafion. Thus, the new design of biopolymeric matrix consisting of XO/fMWCNT/Au-PPD provided better microenvironment for direct electron transfer from catalytic site of the enzyme to the electrode surface by means of conducting tunnels formation through the novel nanobiocomposite layer.

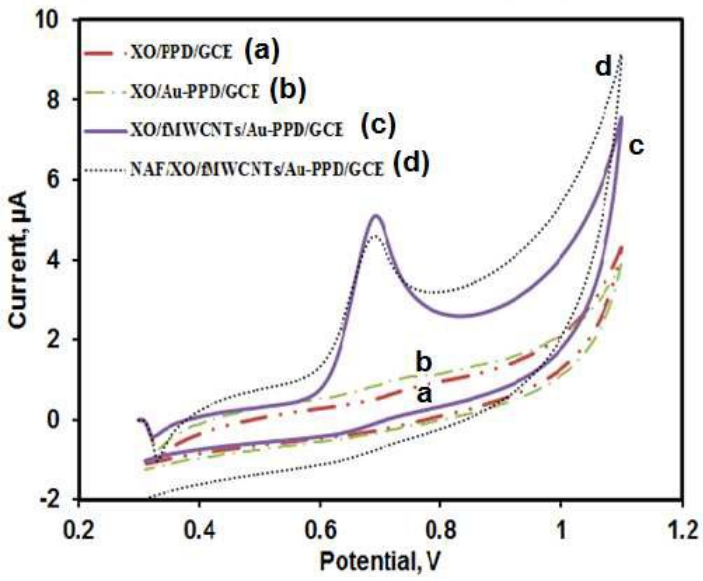

Fig. 4 Cyclic voltammometric response of 50µM xanthine in 50mM Phosphate buffer for XO/PPD/GCE(a),XO/Au-PPD/GCE(b),XO/fMWCNT/Au-PPD/GCE(c), Naf/XO/fMWCNT/Au-PPD/GCE (d). Conditions: potential range: 0.3 to 1, scan rate: 0.1 V s^{-1}. Electrodes: *RE: Ag/AgCl, CE: Platinum wire*

To further prove the electro-catalytic activity of XO/fMWCNT/Au-PPD/GCE, the analytical parameters obtained from the calibration plot using DPV was noted in Table 2. Michaelis-Menten equation applied to electrochemistry is given by:

$$1/Is = 1/I_{max} + [(K_{map} / I_{max}) 1/S] \quad \ldots\ldots\ldots\ldots (2)$$

Where, I_{max} is maximum current value at enzyme–substrate saturation and K_{map} is the substrate concentration at which current response is $I_{max}/2$; that actually represents the enzyme affinity to the substrate. The values of I_{max} and K_{map} were evaluated by non-linear regression analysis using MATLAB 7.1. Highest I_{max} value related to optimum enzyme activity was achieved by the sensor design of XO/fMWCNT/Au-PPD/GCE (showed in table 2). The conservation of native structure of enzyme increased electroactive surface improving performance of the transducer. Since, enzymatic turnover number increased proportionately with the ratio of I_{max} to K_{map}, the optimum design was considered on the basis of higher value of I_{max}/K_{map}.[7,11,16] Nanostructure variation of immobilization matrix could be responsible for increase of active surface area for enzyme binding that could further enhance I_{max}/K_{map} value. The advantages of gold doping in PPD film was clearly noted in table 2. Enzymatic efficiency (I_{max}/K_{map}) was enhanced to nineteen fold for XO/Au-PPD/GCE as compared to XO directly absorbed on PPD film (XO/PPD/GCE), whereas it could increase only two times when AuNP electrodeposited separately onto the PPD film (XO/Au/PPD/GCE). The linear range sensitivity (LRS) of the XO/Au-PPD increased to 55.5 folds due to unique microspheric nanostructure of Au-PPD film that could enhance the active surface area for enzyme binding. The defects of functionalized MWCNT promoted fast electron transfer through the matrix. The electrodeposition of highly conducting fMWCNT on the Au-PPD film enhanced the sensitivity even in nanomolar range, leading to lower LOD (limit of detection) for xanthine detection i.e. 12 nM. The covalent

379 interaction of XO-NH_2 with the $–COO^-$ group of fMWCNT could also stabilize the enzyme
380 loading and hence effectively achieved a turnover number of 2.7 compared to that obtained by
381 XO/Au-PPD/GCE. Though, nafion is commonly used to reduce the interference of ascorbic acid
382 and uric acid in real samples, coating of nafion reduced the enzyme affinity, denatured the
383 enzyme and thus reduced current response.[15,28] The sensitivity of the nafion coated sensor design
384 (Naf/XO/fMWCNT/Au-PPD/GCE) was observed to be lower than that achieved without nafion
385 coating .

386 **Table 2** Analytical parameters obtained from xanthine calibration curve for different modified
387 electrodes.

Modified electrode	I_{max} (μA)	K_{map} (μM)	I_{max}/K_{map} nA/μM	LRS (nA/μM)	LOD (μM/μA)	Range (μM)
XO/PPD/GCE	1.4645	218.136	6.714	1.56	1.2	100-400
XO/Au/PPD/GCE	7.8549	611.995	12.835	6.8	330.84	10-500
XO/Au-PPD/GCE	9.738	74.265	131.125	86.6	1.03	5-50
XO/fMWCNT/Au-PPD/GCE	**43.464**	**122.879**	**353.715**	**991.8**	**0.012**	**0.01-35**
Naf/XO/fMWCNT/Au-PPD/GCE	37.174	142.658	225.817	187.8	5.667	0.5-50

388

389 3.5 *Characterization of modified electrode by FESEM, AFM, FTIR, XRD*

390 Fig. 5a & b displays the FESEM image of successful electro-deposition of fMWCNT
391 onto the Au-PPD surface and XO/fMWCNT/Au-PPD/GCE respectively. The XO molecules
392 were aggregated on the surface of fMWCNT through peptide bond (Fig. 5b). Successful
393 incorporation of XO enzyme on the fMWCNT/Au-PPD changed FTIR spectra (Fig. 5c)

394 significantly showing characteristic bands of polypeptide. The IR spectra of XO/fMWCNT/Au-
395 PPD showed two distinguishable absorption peaks at 1685 and 1570 cm^{-1} for amide I and amide
396 II vibrations of peptide bonds whereas a broad absorption peak at 3480 cm^{-1} peak was attributed
397 for N-H stretching of amide or free amino groups present in the protein backbone. Fig 5d
398 displays the 3D AFM images of XO/fMWCNT/Au-PPD done in tapping phase in 1μm scale. A
399 mesh like porous structure was observed after immobilization of XO on electro-deposited surface
400 of fMWCNT (Fig. 5d). The "cavities" or "holes" on the fMWCNT-modified film might also be
401 helpful for substrates or small inorganic ions in buffers to move into or out of the films, thus
402 improving the electro-catalytic performances. The surface area of the PPD and Au-PPD image
403 was calculated by NanoScope analysis software version 1.4. For Au doped PPD film it was
404 76.4μm^2, whereas same for only PPD film was 4.39 μm^2 (images shows in supplementary
405 documents S Fig 3). The huge change could be possible due to gold nanocluster deposition in
406 Au-PPD film (S Fig 3 a, b). The roughness and depth of XO/fMWCNT/Au-PPD/GCE was
407 calculated to be 32.9±1.3 nm and 21.6±0.8 nm (S Fig 3c).

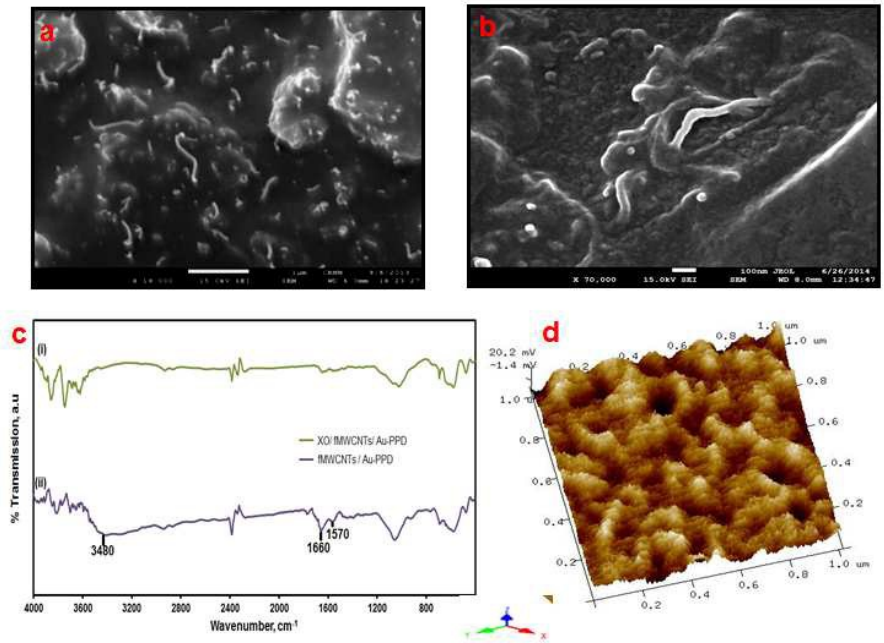

Fig. 5 FESEM images of (a) fMWCNT/Au-PPD and (b) XO/fMWCNT/Au-PPDf; (c) FTIR spectra of modified electrode fMWCNT/Au-PPD/GCE (i), XO/fMWCNT/Au-PPD/GCE (ii); (d) Tapping mode AFM phase images of XO/fMWCNT/Au-PPD;

3.6 Electrochemical Characterization of the modified electrode

Electrochemical impedance spectra (EIS) was performed at each stage of modification of electrode to analyze the change of electrical properties at the interface due to characteristic change in interface at frequency between 0.01Hz to 1MHz at applied potential of 0.28V (anodic peak potential for $K_3Fe(CN)_6$/ $K_4Fe(CN)_6$ with modified electrode). Nyquist plot of different layers of modification in Fig. 6A shows change of charge transfer resistance (Rct) value. The R_{ct} and parallel double layer capacitance (Cdl) varied at higher frequency range that represented a semicircle structure of the spectra while at lower applied frequencies, straight line represented the Warburg-diffusion impedence (Zw) indicating diffusion control charge transfer process. The parameters for surface variation were obtained by fitting the Randles equivalent circuit at the

higher frequency as well as lower frequency range. R_s was related to the uncompensated solution resistance which remained almost constant. The electron transfer resistance (R_{ct}) value for the bare GCE, PPD/GCE, Au-PPD/GCE, fMWCNT/Au-PPD/GCE, XO/fMWCNT/Au-PPD/GCE, electrodes have been obtained as 3.481, 2.298, 0.0851, 64.798, 4.645 KΩ respectively. The electron transfer resistance decreased due to polymerization of OPD that forms a thin conducting polymer matrix (PPD/GCE). The novel Au-PPD film provided 27 times lesser R_{ct} value than PPD/GCE suggesting that the thin film of Au-PPD had higher conductivity than only polymeric film of PPD due to the presence of Au nanoclusters in Au-PPD film. The R_{ct} value increased after electro-deposition of fMWCNT owing to the electrostatic repulsion of negative charge of electrode surface and anions in the solution [$Fe(CN)_6^{3-}$/$Fe(CN)_6^{4}$]. Further reduction of R_{ct} value could explain the successful immobilization of enzyme onto the fMWCNT/Au-PPD/GCE surface.

Fig. 6B depicts Bode phase angles and Fig. 6C represents Bode amplitude plots for bare GCE, PPD/GCE, Au-PPD/GCE, fMWCNT/Au-PPD/GCE, XO/fMWCNT/Au-PPD/GCE. In Fig 5b, the PPD/GCE and Au-PPD/GCE showed lower phase angels such as 43.17° and 31.2° compared to bare GCE (56.13°) indicating increased charge transfer rate at the electrode surface due to presence of gold doped polymer composite film. The fMWCNT/Au-PPD/GCE showed phase angle of 75.68° at low frequency (1.3Hz), indicating ideal capacitive behaviour due to electro-deposition of negatively charged fMWCNT; which further moved to 56.7° at 56.7Hz after enzyme immobilization. The change of phase angle pattern was facilitating charge transfer reaction on XO/fMWCNT/Au-PPD/GCE. In the frequency range from 10^5 to 10^4 Hz, the phase angles approached zero and the |Z| value was almost constant, indicating the same solution resistance (R_s) for all the modification stages of GCE; the R_{ct} value also decreased with

modification of electrodes, thus facilitated electron transfer.[11] In order to calculate the electron transfer rate constant k_0 (data shown in Table 3), Equation 3 was applied at different steps of electrode modification.

$$R_{ct} = RT / (nF)^2 A k_0 C; \quad \text{--- (3)}$$

Where, C is the molar concentration $[Fe(CN)_6^{3-}/Fe(CN)_6^{4}]$ in solution. The calculated k_0 value from the equivalent Randle circuit model was smaller than any previously reported sensing system[27,30].

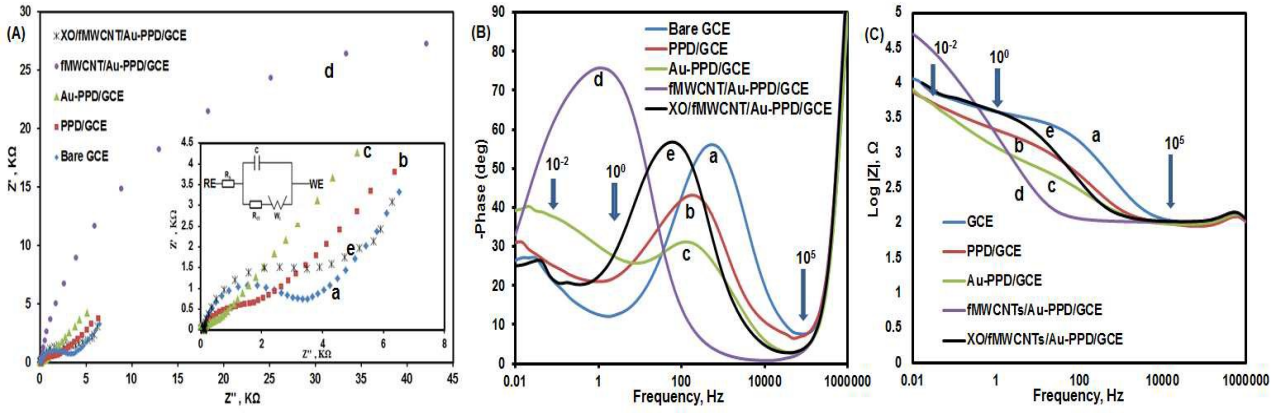

Fig. 6 (A) Nyquist, (B) Bode Phase and (C) Bode amplitude plots of Electrochemical impedance spectra of each step of modifications of XO/fMWCNT/Au-PPD/GCE; (A, inset) shows the equivalent Randle circuit for fitting the circuit of the modified enzyme electrode. The curves represent the results obtained for bare GCE(curve a), PPD/GCE (curve b), Au-PPD/GCE (curve c), fMWCNT/Au-PPD/GCE (curve d), XO/fMWCNT/Au-PPD/GCE (curve e), in 5mM of $[K_3Fe(CN)_6/ K_4Fe(CN)6]$ within frequency range of 1 MHz to 0.01 Hz at constant potential of 0.28V with modulation amplitude 0.01mV using Ag/AgCl as standard RE and Pt wire as CE.

Table 3 Change of impedance values (Rct and k_0) for each step of modification determined from equivalent circuit models

Modified electrode	Rct, Kohm	K_0(cm/s)	Phase angle (^{o}) @frequency
Bare GCE	3.481	2.16E-07	56.133 @543Hz
PPD/GCE	2.298	3.28E-07	43.175 @175.8Hz
Au-PPD/GCE	0.0851	8.85E-06	31.2 @121Hz
fMWCNT/Au-PPD/GCE	64.798	1.16E-08	75.68 @1.3Hz
XO/fMWCNT/Au-PPD/GCE	4.645	1.62E-07	56.7 @50.65Hz

The active surface area of the modified fMWCNT/Au-PPD/GCE electrode was determined by performing CV in the range of -0.5 to 0.6V for 1mM $K_3Fe(CN)_6$ in 0.1M KCl and the slope of the Ip versus υ curve was obtained by varying scan rate from 10mV to 200mV. The active surface area was calculated following Randles-Sevcik equation(4) for reversible process.[11]

$$I_p = (2.69X10^5)n^{3/2}A_c D_r^{\frac{1}{2}} v^{\frac{1}{2}} C \quad \ldots\ldots\ldots\ldots (4)$$

Where I_p refers to the anodic peak current (A), n the number of electrons transferred, A the active surface area (cm^2), D_r diffusion coefficient ($cm^2\ s^{-1}$), υ the scan rate ($V\ s^{-1}$) and C denotes the concentration of the analyte ($mol\ cm^{-3}$), i.e. 1mM $K_3Fe(CN)_6$. For 1mM $K_3Fe(CN)_6$ in 0.1M KCl electrolyte, n=1, C=1 and D_r= 7.6 X 10^{-6} $cm^2\ s^{-1}$ [42]. The linear slope of 3X10^{-5} $A/(V\ s^{-1})$, the active surface area is 0.403cm^2.

The average surface coverage (Γ*) of XO enzyme on the fMWCNT/Au-PPD modified glassy carbon electrode was estimated according to the following equation (5) of Brown-Anson model (Dhyani, Ali, Pandey, Malhotra, & Sen, 2012). I_p (μA) =n^2F^2 Γ* υA/4RT …….. (5)

Where, n denotes number of electron transfer; A area of electrode surface; F the Faraday constant; R universal gas constant; T temperature in Kelvin and υ scan rate. The value of Γ* was calculated from the slope of the I_p versus υ plot and the average surface coverage by XO molecules was about 4.37X 10^{-5} M cm^{-2} under the saturated adsorption conditions, indicating a sub-monolayer of enzyme immobilized on the modified electrode surface that was very large compared to the previous report i,e 7.62X10^{-12} M cm^{-2} of XO immobilized on laponite nanoparticles modified GEC electrode.[27]

3.7 Electrochemical Studies of XO/fMWCNT/Au-PPD/GCE

3.7.1 Influence of pH

The redox potential of an electrochemical reaction depends on the solution pH that indicates the participation of proton in the redox reaction. The influence of buffer pH was displayed in Fig. 7a in the pH range of 5.0 to 9.0 in 50mM potassium phosphate buffer. CV was performed with 5.0X10^{-5}M of xanthine at a scan rate of 100mVs^{-1}. The redox potential (E_p) shifted to negative direction i.e less positive value with increasing the pH from 5 to 9. The linear regression equation $E^{0'}$ = 1081.7-53.33pH was obtained with correlation coefficient of 0.9946 (inset of fig 6a). Since, the value of slope was -53.33 mV pH^{-1} i.e. approximately close to the theoretical value of -59 mV pH^{-1} (Nernstian case); suggested that the number of e^- transfer is equal to the proton coupled with the redox process on the modified electrode surface. The buffer pH= 7 was chosen for further electrochemical analysis owing to the highest peak current for enzymatic oxidation. Since pKa of xanthine is 7.7 and 11.9, it is in slightly positive charged at pH 7. Whereas XO enzyme (pKa=4.2) was negatively charged at pH of electrolyte 7.0. The

active site of XO having Gly-COOH, was responsible for nuclophilic attraction on C8 of xanthine molecule. A stable enzyme-substrate complex was formed by reduction of fully oxidized form of XO-Mo(VI). A water molecule was attributed to oxidize xanthine into the enol tautomer of uric acid, that further reform to keto tautomer of uric acid. The reduced XO-Mo(IV) form of enzyme was further oxidized by two-electron transfer in the electrochemical reaction. As there were no alterations in the peak potentials with respect to the p*K*a values it could be concluded that the protonation reaction was not a rate determining step in the electrochemical oxidation processes. Thus like other FAD-containing flavoenzyme, transfer of two protons was accompanied with two electrons during the electrochemical reaction onto the XO/fMWCNT/Au-PPD/GCE electrode surface and the electrochemical reaction could be described as below:

$$\text{Xanthine} + \text{XO-FADH}_2 \longleftrightarrow \text{Uric acid} + \text{XO-FAD} + 2\,e^- + 2\,H^+ \text{----------(6)}$$

$$2e^- \longrightarrow \text{Working electrode ---------- (7)}$$

3.7.2 Influence of Scan rate

The kinetics of the electrode reactions were investigated by studying the effects of scan rate(υ) on the anodic peak currents(I_p) for xanthine at XO/fMWCNT/Au-PPD/GCE (Fig. 7b). The peak current of $5.0X10^{-5}$ M xanthine increased linearly between 10 and 200mV s-1 and this indicated a typical diffusion controlled process and the equation could be expressed as follows: $I_p=6.5817\ \upsilon^{1/2} - 0.0295$; $R^2 = 0.9842$. In addition, there was a linear relationship between log I_p and log υ with slope of 0.52 that was close to the theoretical value of 0.5 for diffusion controlled process[40,41] given by $\log I_p = 0.5203 \log \upsilon + 0.832$; $R^2 = 0.989$.

The redox peak potential shifted linearly towards positive value with increasing scan rates, corresponding to the following relation: $E_p = 0.0428 \log \upsilon + 0.7658$ with R^2 value 0.9614.

521 According to Laviron[40,41] for irreversible reaction process, E_p is calculated by the following
522 equation:

523 $$E_p = E^{o'} + \left(\frac{2.303\,RT}{\propto nF}\right)\log\left(\frac{RT\,k^o}{\propto nF}\right) + \left(\frac{2.303\,RT}{\propto nF}\right)\log \upsilon \quad \ldots\ldots\ldots\ldots (8)$$

524 Where $\propto$ is the transfer coefficient, k^o is the standard heterogeneous rate constant of the reaction,
525 n is the number of electron transferred through the electrode, υ is the scan rate and $E^{o'}$is the
526 formal redox potential. Other symbols are universal standard R= 8.314 J K^{-1}, F=96480 C mol^{-1},
527 T= 298K. The value of $\propto n$ calculated as 1.382 from the slope of E_p vs log υ i.e., 0.0482. The α
528 value was calculated from the Bard and Faulkner (2004) equation (9): [4]

529 $$\alpha = \frac{47.7}{E_p - E_{p/2}}\,mV \quad \ldots\ldots\ldots\ldots\ldots\ldots (9)$$

530 Where $E_{p/2}$ is defined as the potential where current is the half of the peak current. For our
531 system α is 0.596. Thus the number of electron transferred (n) during the oxidation of xanthine
532 was calculated as 2.32 ~ 2.

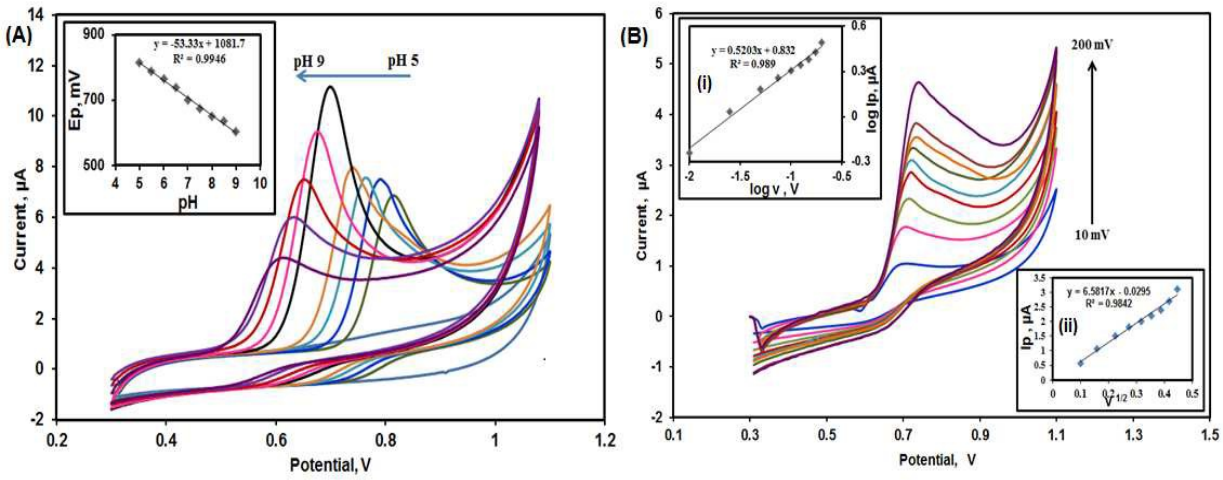

533

534 **Fig. 7** Cyclic voltammograms of modified electrodes in presence of 5.0X10^{-5}M of xanthine in
535 50mM phosphate buffer; (A) at different pH range of 5.0 to 9 at a scan rate of 100mVs^{-1}. (Inset:

plot of $E^{o'}$ vs pH) ; (B) at different scan rates of 10, 25, 50, 75, 100, 125, 150, 175, 200mVs^{-1}; inset: i) dependence of the logarithm peak current on logarithm of scan rate (R^2 = 0.995); another ii) calibration plot for Ip versus $\upsilon^{1/2}$. Conditions: potential range: 0.3 to 1, scan rate: 0.1 V s^{-1} Electrodes- WE: *XO/fMWCNT/Au-PPD/GCE, RE: Ag/AgCl, CE: Platinum wire*

3.8 *Evaluation of performance parameters of the proposed xanthine biosensor*

Fig. 8 displays the differential pulse voltammetric (DPV) response for oxidation of xanthine on the modified electrode for a wide range of xanthine concentration of 0.01-300µM. DPV was conducted in 50mM potassium phosphate buffer, pH 7 with 50mV pulse amplitude and step potential of 10mV in the range of 0.4 to 1.0 V. The oxidation potential of xanthine was shifted towards higher potential with addition of increasing concentration of xanthine.[17] The xanthine standard curve was linear for 0.01 to 0.250 µM given by the equation: Ip (µA) = 0.9979[xan] +0.0114 (R^2=0.99); 0.1 to 35 µM with Ip (µA) = 0.2559[xan] +0.0857 (r2= .998) and for 35 to 200 µM with Ip (µA) = 0.0999[xan] +6.392(R2= 0.982). The limit of detection (LOD= [(3*SD of blank) /slope] and limit of quantification (LOQ= [(10*SD of blank)/slope]) were calculated as 12nM and 40nM respectively (for lowest range of calibration curve) based on S/N=3. The lowest detection limit of the new sensing system compared very well with reported xanthine sensors i.e. modified glassy carbon electrode coated with graphitized mesoporous carbon (0.388µM)[10] , XO immobilized on laponite NP modified electrode (0.01 µM)[27], P(GMA-co-VFc)/MWCNT/XO (0.12 µM)[24], Naf/XO-CD/pAuNP/SWNT/GCE (0.04 µM)[28], DNA–polyaniline (PAn) complex Langmuir–Blodgett film (30nM)[17] (see note at bottom of Table 1 for abbreviations).

The analytical performance of the proposed sensor was better than any of the previously reported xanthine sensors with respect to the stability. The long-term storage stabilities of the

proposed modified XO electrode were tested every week for six months. After each experiment, the electrode was washed with reaction buffer and stored in phosphate buffer at 4◦C. The stability was calculated using the formula:

$$\%\text{Stability} = 100 - [(I_n - I_o)/ I_o] \times 100 \quad \ldots\ldots\ldots\ldots (10)$$

where I_0 is the obtained current in first day and I_n is the obtained current on n^{th} day. It was observed that the modified electrode could be used comfortably up to 180 times. The electrode retained more than 91% activity after storing it for 130 days (in Fig.S4). The higher stability of XO/fMWCNT/Au-PPD/GCE than previous reports [4,10,17,23-31] might be due to the strong covalent bonding of carboxylated MWCNT and free $-NH_2$ of the enzyme that prevented leakage of enzyme from the electrode surface.

The biosensor showed highest sensitivity of 14.03 $\mu A\ \mu M^{-1}\ cm^{-2}$ towards xanthine detection. The reproducibility of the sensory system was investigated by modification of four glassy carbon electrodes and observing their anodic response towards 50μM xanthine by five repeat measurements. The peak current was determined five times with the same electrode (within batch) and four different electrodes (between batches). The response for same fish extract showed almost consistent results of xanthine content within and between batches i.e. coefficient of variation (CV) were <1.93 and <3.08 % (Table S1). The repeatability of the biosensor was analyzed at 50μM xanthine and the relative standard deviations for six determinations were 2.1% and 2.8%, respectively.

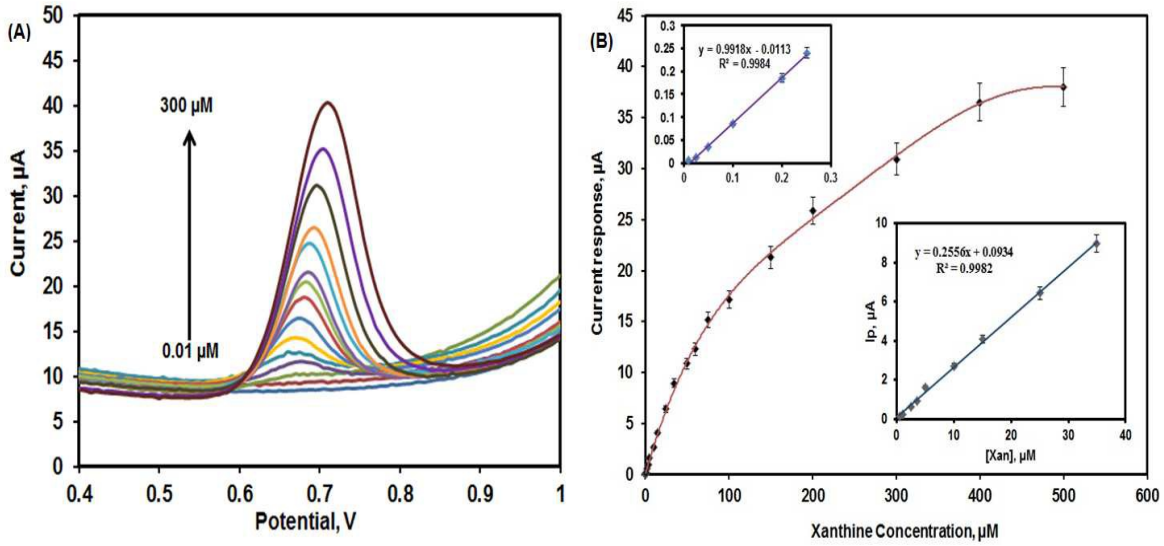

577

578 **Fig. 8** (A) Differential pulse voltammetric response of different concentration of xanthine such
579 as 0.01, 0.1, 0.5, 1, 2.5, 5, 10, 25, 50, 75, 100,150, 200, 300 in 50mM phosphate buffer, pH7; (B)
580 the current response of xanthine in the range of 1-300µM, inset: calibration curve of the linear
581 range of 0.01 to 35 µM and 0.5 to 35 µM; Conditions: potential range: 0.3 to 1, scan rate: 0.1 V
582 s^{-1} in 50mM phosphate buffer using three electrode system of WE: *XO/fMWCNT/Au-PPD/GCE,*
583 *RE: Ag/AgCl, CE: Platinum wire.*

584

585 *3.9 Selectivity of xanthine biosensor*

586 The selectivity of the immobilized enzyme electrode was evaluated by its ability to protect
587 the sensor from other electroactive interfering compounds that might be present in the real
588 samples. The specificity of the biosensor was monitored in presence of some interfering
589 chemicals (1mM) such as hypoxanthine, inosine, inosine monophosphate, uric acid (UA),
590 ascorbic acid (AA), oxalic acid, L-cysteine, glucose, sucrose, theobromine, theophylline. Since,
591 co-electro-oxidation of potential interferences such as AA and UA is one of the major problems

592 in the amperometric detection of analytes, DPV was performed owing to its ability to give
593 distinct oxidation potentials for each substances. The interference of the above reagents (1mM)
594 was investigated by monitoring the DPV response in the range of 0.3 to 1.0 V. It could be seen
595 from Fig. 9 that there was no interference for the common interfering compounds near the
596 oxidation potential of xanthine, i.e. 0.625-0.725V. Uric acid depicted an oxidation potential at
597 0.29V and ascorbic acid oxidized at 0.05V; both the oxidation potential exhibit far away from
598 the target potential of interest, i.e. nearly 0.65V. Most importantly, the enzyme electrode did not
599 show any response towards the common electroactive biologically important molecules such as
600 ascorbic acid (AA) (1mM) and uric acid(UA) (0.5mM) in the potential scan range of 0.4 to 1.0
601 V. Since active form of anionic XO (pKa = 4.2± 0.1) was immobililized on carboxylated
602 MWCNT at the electrode surface, the modified XO/fMWCNT/Au-PPD electrode was negatively
603 charged and could repel negatively charged interfering substance (such as AA, UA etc) present
604 in the real sample. Thus the response for electroactive anions present in biological media
605 declined to a great extent.

606 Since, it also known that PPD depicts well permeability and permselectivity towards AA.
607 The apparent permeability of AA for XO/fMWCNT/Au-PPD was calculated as 2.34% using the
608 following equation(11).[16]

609

$$P(AA)\% = \frac{I_{AA}(1mM)\text{at PEC/GCE}}{I_{AA}(1mM)\text{at bare GCE}} \times 100\% \quad \text{--------- (11)}$$

610

611 Where, I_{AA}(1mM)at PEC/GCE was determined as the nanoampere value at the fixed
612 potential 0.65V for modified polymer enzyme composite (PEC).

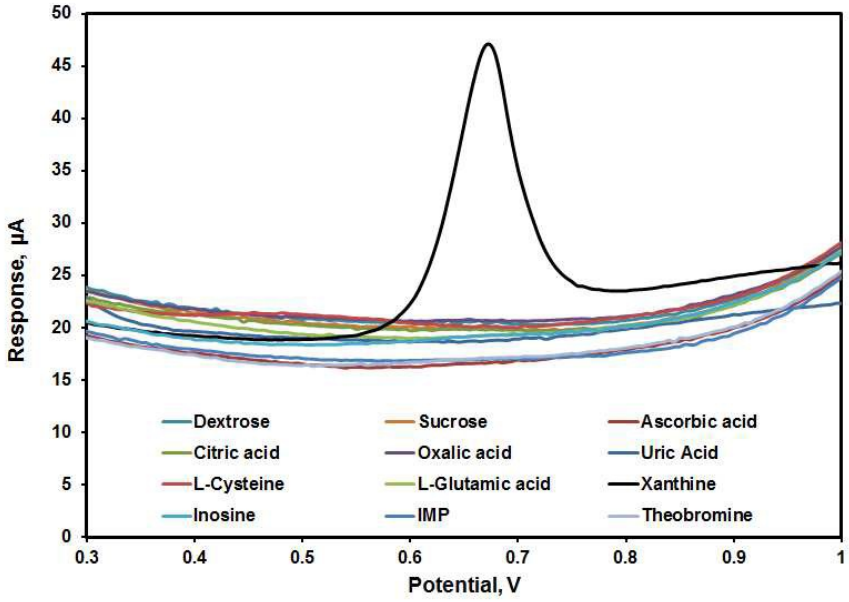

Fig. 9 DPV response for interfering substances (1mM) present in biological media. DPV response of some interfering substances. Conditions: potential range: 0.3 to 1, scan rate: 0.1 V s^{-1} in 50mM phosphate buffer using WE: *XO/fMWCNT/Au-PPD/GCE, RE: Ag/AgCl, CE: Platinum wire*.

3.10 Real sample analysis

Freshness of fish could be monitored by determination of xanthine during its storage. The level of xanthine in blood serum and urine are of importance in clinical diagnosis. Hence the proposed biosensor was tested with human serum and urine samples as well as fish extract. The accuracy of the proposed sensor was investigated by standard addition method to determine xanthine content in real samples. In this method, additions of standard xanthine solution were made several times to the each sample. The results were compared in Table 4 with standard HPLC based method. The xanthine values obtained by the present biosensor (y) matched with standard HPLC data with good correlation (y= 0.9984x + 0.0124, r = 0.998, significant at 1% level), showing high accuracy of the proposed method. Table 4 represents a good agreement

between biosensor and HPLC methods, indicating that the present method could be used for real samples analysis. Spoilage of fish could be monitored by registering the concentration of xanthine with storage time. The spoilage rate of fish was determined by storing it in $0^{o}C$, $-20^{o}C$ temperature and monitoring the xanthine content in 30ul of fish extract. The response increased abruptly with increasing storage temperature (Table 5).

Table 4 Determination of xanthine in real samples using XO/fMWCNT/Au-PPD/GCE.

Sample	Added (μM)	Found (μM) by Biosensor	Recoveries (%)	Original (μM) by HPLC	Relative Error (%)	RSD (%)
Fish sample 1	0 (30μl)	4.8	101.05	4.86	1.235	1.597
(Labio	5	9.75	99.08	9.84	0.915	0.785
rohita)	10	14.82	98.66	15.021	1.338	1.617
Fish sample 2	0 (30μl)	3.609	98.79	3.653	1.204	1.269
(Lates	5	8.458	98.44	8.592	1.560	0.993
calcarifer)	10	14.019	101.40	13.825	1.403	1.561
Blood serum	0 (50μl)	2.514	98.67	2.514	1.334	3.813
	5	7.805	102.68	7.960	1.947	1.667
	10	12.537	99.82	12.56	0.183	1.518
Urine	0 (50μl)	0.301	103.44	0.291	3.436	3.32
	5	5.230	97.74	5.351	2.261	1.68
	10	10.463	101.85	10.273	1.849	0.893

* All the experimental data showing P value (n=5)<0.05

635

636 **Table 5** Determination of xanthine concentration in fish extracts (*Labio rohita)* solution stored at
637 different temperature

Storage Time (day)	Storage Temperature	
	-20°C	0°C
0	3.034±0.23	3.109±0.34
1	3.612±0.27	5.012±0.43
3	4.032±0.31	9.245±0.61
5	6.258±0.53	15.179±0.76
7	7.676±0.68	30.810±1.03

638

639

640 ## 4. Conclusions

641 A novel interference free xanthine biosensor was successfully fabricated. The most
642 important achievement of this study was rapid formation of an ultrathin Au decorated PPD film
643 (thickness-178.2±12nm) having good permselectivity and permeability by one step
644 electrodeposition. EIS study depicted that nanospheric structure of gold doped PPD film
645 enhanced the conductivity when compared with only PPD film. The large number of hydroxyl
646 and carboxyl groups in fMWCNT provided increased active surface area for loading higher
647 amount of xanthine oxidase enzyme and more surface energy that led to the favourable
648 conformational change of protein for direct electron transfer between active site of enzyme to the

underlying electrode. The covalent interaction of the enzyme enhanced enzyme stability on the modified electrode and retained its catalytic activity up to 6 months. The sensor depicted good catalytic activity (I_m/k_m) and higher substrate affinity (K_m=0.123mM). The oxidation of xanthine onto to the modified electrode surface was found to be irreversible and diffusion controlled process. The newly designed XO/fMWCNTfMWCNT/Au-PPD/GCE sensor exhibited good electrode characteristics including high sensitivity (14.03 μA μM^{-1} cm^{-2}) with low LOD of 12nM, rapid response (5s). A wide range of linear calibration curve was obtained for 0.01-200 μM of xanthine (R^2=0.99). The coefficients of variation for reproducibility were found to be only 1.9% and 3.1 within and between the assays. It also exhibited good repeatability of 2.1%. Furthermore, the XO/fMWCNT/Au-PPD/GCE showed excellent selectivity towards xanthine in the presence of interfering agents such as ascorbic acid, glucose and uric acid. The proposed sensor also showed good correlation (r=0.998) with standard HPLC data having high recovery rate 97-101%. Hence, the sensor could be useful for rapid analysis of xanthine in real samples such as blood, urine, tissue In addition, this novel immobilization matrix could be extended to other enzyme for fabrication of efficient biosensors.

Acknowledgement

The authors are very much thankful to CRNN, University of Calcutta to provide the facility of SEM, FESEM, TEM and DBT-IPLS for AFM facility.

Reference

1 G. Volpe and M. Mascini, *Talanta,* 1996, 43, 283-289.

2 V. Venugopal, *Biosens. Bioelectron.,* 2002, 17 147–157.

3 N. Cooper, R. Khosravan, C. Erdmann, J. Fiene and J.W. Lee, *J. Chromatogr. B*, 2006, 837, 1–10.

4 R. Devi, M. Thakur and C.S. Pundir, *Biosens. Bioelectron.,* 2011, 26, 3420–3426.

5 L.D. Mello and L. T. Kubota, *Food Chem.,* 2002, 77, 237–256.

6 A. J. Bard and L.R. Faulkner, Electrochemical Methods Fundamentals and Applications, 2nd ed., Wiley, New York, 2004.

7 P. Q. Pandey, S. K. Arya, Z. Matharu, S. P. Singh, M. Datta and B.D. Malhotra, *J. Appl. Polym.Sci.,* 2008, 110, 988–994.

8 Rajesha, T. Ahuja and D. Kumar, *Sens. Actuators B,* 2009, 136, 275–286.

9 W. Fenga and P. Ji, *Biotechnol. Adv.,* 2011, 29, 889–895.

10 R. Thangaraj and A.S. Kumar, *Anal. Methods,* 2012, 4, 2162-2171.

11 T. Ghosh, P. Sarkar and A. P.F. Turner. *Bioelectrochemistry*, 2015, 102, 1–9.

12 M. Ates, *Mater. Sci. Eng.: C*, 2013, 33, 1853–1859.

13 L. Xia, Z. Wei and M. Wan, *J. Colloid Interf. Sci.,* 2010, 341, 1–11.

14 P. Gajendranand and R Saraswathi, *J. Phys. Chem. C*, 2007, 111, 11320-11328.

15 E. Turkmen, S. Z. Bas, H. Gulce and S. Yildiz, *Electrochim. Acta,* 2014, 123, 93–102.

16 A. Khan and S. A. Ghani, *Biosens. Bioelectron.,* 2012, 31, 433–438.

17 L. Zou, Y. Li, S. Cao and B. Ye, *Talanta*, 2014, 129, 346-351.

18 S. A. Ansari and Q. Husain, *Biotechnol. Adv.,* 2012, 30, 512–523.

19 K. Ding, H. Jia, S. Wei and Z. Guo, *Ind. Eng. Chem. Res.,* 2011, 50, 7077–7082.

694 20 R. Devi, S. Yadav and C.S. Pundir. *Colloid Surfaces A,* 2012, 394, 38–45.

695 21 P. Xu, X. Han, B. Zhang, Y. Du and H-L. Wan. *Chem. Soc. Rev.,* 2014, 43, 1349 22 A. B.

696 Moghaddam, T. Nazari, J. Badraghi and M. Kazemzad, *Int. J. Electrochem. Sci.* 2009, 4, 247–

697 257.

698 23 R. Devi, S. Yadav and C. S. Pundir. *Analyst,* 2012, 137, 754–759.

699 24 M. Dervisevic, E. Custiuc, E. Çevik and M. Şenel. *Food Chem.,* 2015, 181, 277–283.

700 25 Ü. A. Kirgöz, S. Timur, J. Wang and A. Telefoncu, *Electrochem. Commun.,* 2004, 6, 913–

701 916.

702 26 M. Çubukçu, S. Timur and Ü. Anik, *Talanta,* 2007, 74, 434–439.

703 27 D. Shan, Y-N. Wang, H-G. Xue, S.Cosnier and S-N. Ding, *Biosens. Bioelectron.,* 2009, 24,

704 3556−3561.

705 28 R. Villalonga, P. Díez, M. Eguílaz, P. Martínez, and J M. Pingarrón, *ACS Appl. Mater.*

706 *Interfaces*, 2012, *4* , 4312–4319.

707 29. L. Zhang, J. Lei, J. Zhang, L. Ding and H. Ju, *Analyst,* 2012, 137, 3126-3131.

708 30 R. Devi, S. Yadav, S. Nehra and C.S. Pundir. *J. Food Eng.,* 2013, 115, 207–214.

709 31 S. Sadeghi, E. Fooladi and M. Malekaneh, *Anal. Biochem.,* 2014, 464, 51–59.

710 32 S. Goyanesa, G. R. Rubiolo, A. Salazard, A. Jimenod, M. A. Corcuerad and I. Mondragon,

711 *Diam. Relat. Mater.*, 2007, 16, 412–417.

712 33 V. Datsyuk, M. Kalyva, K. Papagelis, J. Parthenios, D. Tasis, A. Siokou, I. Kallitsisand and

713 C. Galiotis, *Carbon,* 2008, 46, 833–840.

714 34 J. Zhang, C. Yang, X. Wang and X. Yang, *Analyst,* 2012, 137, 3286–3292.

715 35 H. Chi, B. Liu, G. Guan, Z. Zhang and M.Y. Han, *Analyst,* 2010, 135, 1070–1075.

716 36 S. Bilal and R. Holze, *Electrochim. Acta,* 2007, 52, (5346-5356.

37 U. Olgun and M. Gülfen. *React. Funct. Polym*.,2014, 77, 23–29.

38 L. Zhang, W. Yuan and Y. Yan, *Electrochim. Acta,* 2013, 113, 218–228.

39 T. Li, C. Yuan, Y. Zhao, Q. Chen, M. Wei and Y. Wang, *J. Macromol. Sci. A,* 2013, 50, 330-333.

40 C. Lanzellotto, G. Favero, M. L. Antonelli, C. Tortolini, S. Cannistraro, E. Coppari and F. Mazzei, *Biosens. Bioelectron.*, 2014, 55, 430–437.

40 E. Laviron, *J. Electroanal. Chem. Interfacial Electrochem.,* 1979, 101,19

41 A. L. Eckermann, D. J. Feld, J. A. Shaw and T. J. Meade, *Coord Chem Rev*., 2010, 254, 1769–1802.